Original Research Paper

Spatial Distribution and Evaluation of Heavy Metal Pollution in Soil Based on Three-Dimensional Model and Kriging Interpolation

[1]Baoshun Liu, [1]Yonghong Zhang, [2]Jun Yao and [3]Jian Su

[1]*Department of Civil and Resource Engineering, University of Science and Technology Beijing, China*
[2]*Department of Water Resources and Environment, China University of Geosciences (Beijing), China*
[3]*Guangxi Bossco Environmental Protection Technology Co., Ltd, Guangxi Bossco, China*

Abstract: Soil heavy metal pollution is an important content for soil environmental governance. Based on the three-Dimensional (3D) geological modeling technology and ordinary Kriging method, this study described and analyzed the soil pollution status and spatial distribution characteristics of a site in Zhongshan, Guangxi. The results showed that combining 3D geological model and the Kriging interpolation method can well evaluate soil heavy metal pollution. The 3D geological model showed that the pollutant concentration in soil ranked As>Pb>Mo and the pollution degree decreased gradually from top to bottom. As such, the miscellaneous fill soil layer was the layer that needs to be repaired. In addition, the single-factor pollution level and Nemerow comprehensive index method were used to evaluate the pollution risk of the site. The evaluation results showed that the soil quality was seriously threatened by As and the heavy pollution (Pi>3) accounted for 61.10%. Furthermore, attention should be paid to the potential risk of Pb in the miscellaneous fill layer. This study can provide a 3D visualization method for comprehensive analysis of soil heavy metal pollution and a scientific reference for the formulation and implementation of subsequent site remediation strategies.

Keywords: Soil Heavy Metals, Spatial Distribution, Ordinary Kriging, 3D Geological Modeling

Introduction

Soil is the basic material of human production and the origin of cultural civilization (Gruszecka-Kosowska, 2019). Its development is affected by climate and meteorology (Othmani *et al*., 2015), soil parent rock (Santos-Francés *et al*., 2017), landform, vegetation coverage, and human activities. Behaviors such as land-use change, vegetation destruction, and soil layer destruction caused by human activities can affect the urban microclimate and cause large-scale air, river, and soil pollution (Liu *et al*., 2020a; Sampson *et al*., 2021).

The treatment of heavy metal pollution sites is a common and urgent problem facing the world (Hou *et al*., 2017). Scholars have been assessing soil heavy metal enrichment to quantitatively identify the pollution sources or developing models to predict the impact of heavy metals on industrial operations (Abderrahmane *et al*., 2021; Buaisha *et al*., 2020). Before on-site treatment, based on mastering the spatial distribution of pollutants, it is necessary to evaluate the pollution degree and polluted earthwork at the site.

Spatial interpolation is an important method to simulate the spatial distribution of heavy metals in soil (Zhang *et al*. 2021). It can determine the distribution characteristics of soil heavy metals. Sabet Aghlidi *et al*. (2020) used Kriging technology to interpolate the contents of all analyzed elements for the whole agricultural area of Eghlid County. O'Shea *et al*. (2021) used the natural neighborhood method to approximately determine the Pb content in the area around the sample location. Ahado *et al*. (2021) used ordinary Kriging interpolation to determine the difference and similarity proportional to the distance between stations. Chen *et al*. (2021) interpolated the surface pollutants in the mining area by the Kriging interpolation method. Agyeman *et al*. (2021) evaluated the spatial distribution of PTE in topsoil and subsoil by inverse distance weighted interpolation.

Substantially, multivariate statistics were also used in soil pollution assessment. Nazzal *et al*. (2021) used multivariate analysis and calculation of pollution index to evaluate the concentration of 17 elements in the agricultural soil of Abu Dhabi Emirate, then grouped them. Huang *et al*. (2020) used the Inverse Distance Weighted (IDW) method to create the spatial distribution map of potentially toxic elements and analyzed the sources of As, Pb and Cr by principal component analysis. Currently, topsoil sampling is mostly used in site pollution assessment. It adopts two-dimensional data and lacks 3D model establishment. Since the soil is permeable and the movement speed of pollution is controlled by soil porosity, the lateral and vertical migration of pollutants needs to be considered when conducting site assessments (Barca *et al*., 2021). As a result, it is difficult to fully and accurately understand the geological conditions of underground space, the distribution pattern of pollutants, and the polluted earthworks. If only the surface layer is sampled, it will bring difficulties or even errors to the detailed investigation of the site and the subsequent soil remediation construction.

There used to be an arsenic production workshop in the southwest of Zhongshan County, Guangxi, and ammonium molybdate was produced in the northern workshop. A large number of wastes are piled up randomly without treatment, which has potential As, Mo, and Pb pollution risks to the site and surrounding environment. Therefore, it is necessary to evaluate the pollution degree and estimate the polluted earthwork of the site. It is also urgent to fully understand the pollution status and spatial distribution characteristics of heavy metals in the study area. Based on the borehole sampling data and the establishment of a borehole geological database, a 3D geological model of the site is established.

This study aims to analyze the spatial distribution of soil heavy metals, explain the reasons affecting the spatial distribution of heavy metals and calculate the polluted earthwork. The method in this study can provide a reference for analyzing the spatial distribution of pollutants, provide a theoretical basis and case support for the polluted target control in the study area and realize the three-dimensional visualization of the spatial distribution of pollutants in the horizontal and vertical directions.

Materials and Methods

The workflow of the proposed methodology of the present study is depicted in Fig. 1. The operational workflow diagram of the proposed methodology includes the establishment of the three-dimensional model, Kriging interpolation prediction, and heavy metal pollution evaluation.

Study Area

The site is located in Zhongshan County, Hezhou, Guangxi Province, with typical karst landform characteristics. It is a subtropical monsoon climate and the rainfall is mainly concentrated from April to June. The site to be treated and repaired is about 38547 m². From top to bottom, the soil of the site are Miscellaneous fill (average 1.79m), Silty clay (average 3.62 m), silty clay with gravel sand (average 4.34 m) (artificially accumulated in the quaternary system), and the gravel sand of Pleistocene alluvial-pluvial origin (average 4.46 m). The geological structure of the site is simple. There are no new active faults passing through the site and its vicinity and the regional geological structure is stable. Runoff in the county is divided into Local River runoff and guest water runoff. The main source of river runoff in the territory is atmospheric precipitation. The surface water is mainly from the reservoirs on the northeast and south sides of the site.

Sample Collection

To grasp the spatial distribution of arsenic, plumbum, and molybdenum at the site, drilling sampling is conducted through the principle of combining professional judgment and grid distribution. The accuracy of sampling points in the suspected polluted areas is not less than 20×20 m and that outside other suspected polluted areas is not less than 40×40 m. As shown in Fig. 2, the site has 75 sampling points and can be divided into.

3D Geological Model Construction

A geological database is the basis of 3D geological modeling. Generally, the geological database to be established includes a collar table, survey table, rock table, and assay table (Van Dyke *et al*., 2020; Kasmaee *et al*., 2010; Xiang *et al*., 2019). The tables are associated with "hole_id" and the fields contained in the four tables are shown in Table 1.

The solid model shows the soil layers in three dimensions. On each exploration line section, the boundaries of the same soil layer in the borehole are connected to obtain the stratigraphic interpretation lines. The stratigraphic interpretation lines at different sections are connected bya triangular network to form a stratigraphic solid model. To interpolate the grade of heavy metal pollutants, it is necessary to establish a block model of the site based on the solid model. Typically, the block size in the X and Y planes is 1/3-1/5 of the exploration spacing, and that in the Z direction is 2-3 times the combined sample length (Choudhury, 2015).
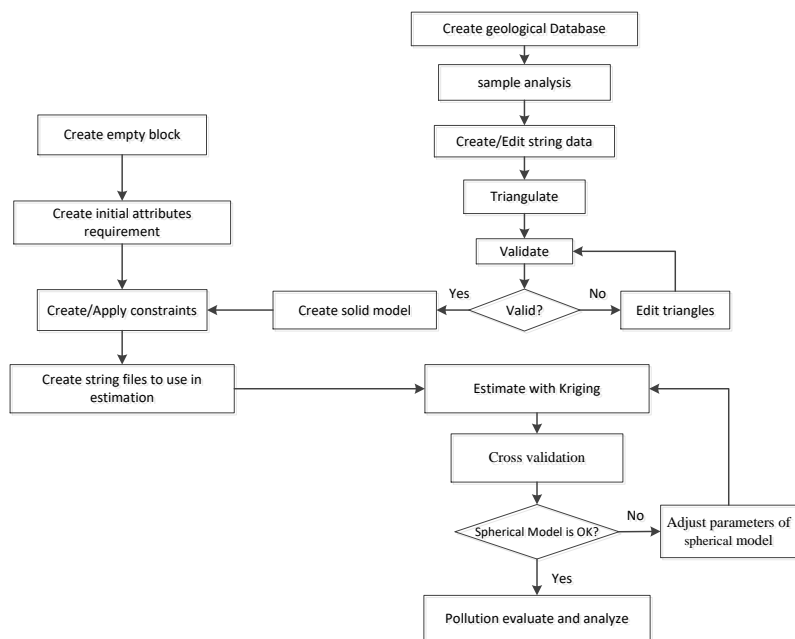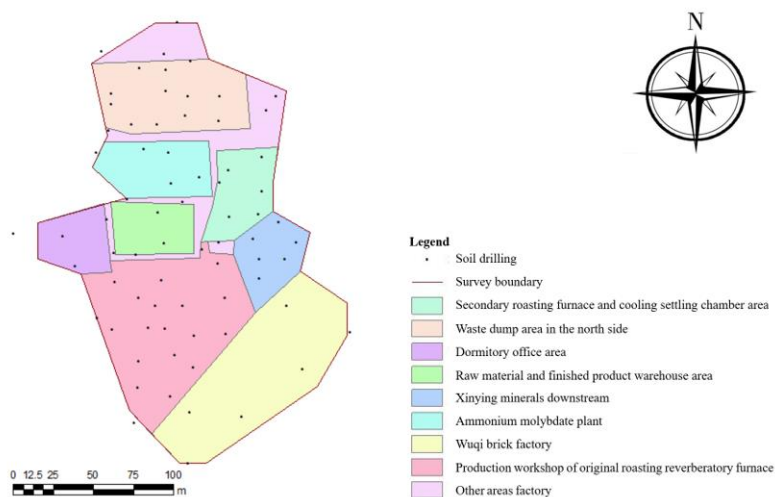
Fig. 1: Study workflow

Fig. 2: Layout of soil sampling

Table 1: Structure of surface geological database

Name	Field					
Collar	Hole_id	Y	X	Z	Max depth	Hole path
Survey	Hole_id	Depth	Dip	Azimuth		
Rock	Hole_id	''	Depth from	Depth to	Rock	
Assay	Hole_id	Sampled	Depth from	Depth to	As, Mo, Pb	

Spatial Variability Analysis

The spatial variation characteristics of elements in the soil can be understood as the relationship between the semi variance and spatial distance. Geostatistical analysis needs to satisfy the second stationary assumption. It is difficult to strictly satisfy the second stationary assumption. Thus it only needs to satisfy the mathematical expectation that the difference between two sampling points at any given distance is 0 and has a finite variance

depending on the spatial position (Breckenkamp *et al.*, 2021; Sauzet *et al.*, 2021; Setiyoko *et al.*, 2020). The experimental semivariogram is the distribution of the semivariogram with a specific lag (Tabesh *et al.*, 2021; Huang and Xie, 2019). The semivariogram is fitted by Surpac to create a continuous model. The fitting function of the semivariogram is:

$$\gamma^*(h) = \frac{1}{2N(h)} \sum_{i=1}^{N(h)} \left[Z(x_i) - Z(x_i + h) \right]^2 \qquad (1)$$

where, $\gamma^*(h)$ is the experimental variogram value; $Z(x_i)$ is the observed value at position i; $Z(x_i+h)$ is the observed value when h is away from x and $N(h)$ is the logarithm of data points separated by h (Barkat *et al.*, 2021; Chaudhry and Sachdeva, 2022).

Based on discrete observations, the theoretical semi-variogram model is used. The spherical, exponential, and Gaussian models fit continuous curves to quantitatively describe the spatial correlation of variables between any points (Fitriani and Sumarminingsih, 2014; Yan *et al.*, 2021). The spherical model is often used to describe soil heavy metal pollution:

$$\gamma(h) = \begin{cases} 0 & h = 0 \\ c_0 + C\left(\dfrac{3h}{2a} - \dfrac{h^3}{2a^3} \right) & 0 < h \leq a \\ c_0 + C & h > a \end{cases} \qquad (2)$$

where, C_0 is the nugget value; a is the range; h is the hysteresis and C_0+C is the sill value.

For geostatistical methods, the most widely used is the ordinary Kriging method developed from the mineral reserves (Coulibaly *et al.*, 2021; Park *et al.*, 2019). The ordinary Kriging method is a geostatistical interpolation method based on spatial correlation variance and is used to find the best linear unbiased estimation (Al-Mamoori *et al.*, 2021; Belkhiri *et al.*, 2020; Hasan *et al.*, 2021). The formula is as follows:

$$Z(x_p) = \sum_{i=1}^{n} \lambda_i Z(x_i) \qquad (3)$$

where, $Z(x_p)$ is an estimate of the variable Z at position x_p; $Z(x_i)$ is a known value of position x_i and λ_i is the weight.

Evaluation of Heavy Metals in Soil

Single-factor index method (Wang *et al.*, 2014) and Nemerow comprehensive index method are used for soil heavy metal pollution assessment:

$$P_i = \frac{C_i}{S_i} \qquad (4)$$

$$P_z = \sqrt{\frac{\left(P_{ivag} \right)^2 + \left(P_{i\max} \right)^2}{2}} \qquad (5)$$

where, P_i is the environmental quality index of the ith pollutant in soil; C_i is the measured concentration of the ith pollutant (mgkg^{-1}) and S_i is the evaluation standard of the ith pollutant (mgkg^{-1}). The greater the index, the higher the accumulation concentration of heavy metals in soil (Qi *et al.*, 2020). P_Z is the Nemerow integrated pollution index; $P_{i\max}$ is the maximum single-factor index value for heavy metals and P_{iavg} is the average value.

Results and Discussion

3D Geological Model of the Site

Through the sampling data of the on-site borehole, the 3D spatial position and shape of the borehole can be visually displayed through the 3D borehole database after the geological database is established by using the Surpac software (Li *et al.*, 2013). On the exploration line profile, different boreholes are respectively surrounded by wireframes according to the miscellaneous fill, silty clay, silty clay with gravel-sand, and gravel sand. A total of four wireframe models are formed on each profile. Wireframes representing the same soil layer on different exploration lines are filled with triangulation nets to form 4 solid models. After the solid model is established, it needs to verify its effectiveness and check whether there is overlap between the triangulation networks. Figure 3 shows the solid model and sampling boreholes of the site after the validity of this article is verified.

The spacing of drilling lines on site is 20×20 m and the max drilling depth is 20 m. According to the drilling layout of the site, the unit block size is determined as $4 \times 4 \times 1$ and $2 \times 2 \times 0.5$ m is the secondary block size.

Statistical Analysis of Data

Traditional statistical analysis is used to determine the basic characteristics of the data and obtain the sampling length to provide a parameter basis for the combined sample length (Ćujić *et al.*, 2017). The average onsite sampling leng this 1.156 m. After calculation and regularization, 1 m integrated samples can well analyze the structure of the variogram.

The statistical results of the integrated samples are shown in Table 2. It can be seen that As, Mo, and Pb all have different degrees of pollution at the site. The average concentrations of pollutants in the entire formation are 1700 mgkg^{-1} (As), 28.27 mgkg^{-1} (Mo) and 1.20 mgkg^{-1} (Pb). Liu *et al.* (2020b) also came to this conclusion when they investigated the surrounding area of the site. Comparing the Coefficient of variation (Cv), it was found that there was significant variation in pollutants, which were 2.55 (As), 5.3 (Mo), and 12.54 (Pb). All are greater than 1.0, which is a strong variation. It shows that the distribution of pollutants at the site is uneven and the soil pollution is greatly affected by human activities, that is, there are behaviors such as pollutant leakage and waste residue stacking in the production process.

The standard deviation in Table 2 varies greatly and the skewness and kurtosis values show that the heavy metal content at the site does not meet the requirements of a normal distribution and an ordinary Kriging unbiased estimate. To ensure that the data does not deviate significantly from the normal (Tziachris *et al*., 2017), the data needs to be preprocessed before calculating the variogram. In this study, the logarithm method is used to complete the data preprocessing. When taking the logarithm, the formula Log_{10} (d1+0.0001) is used. d1 represents the contents of As, Pb, and Mo. After taking the logarithm, the skewness in Table 2 is close to 0 and the kurtosis is close to 3, which meets the normal distribution.

Variogram Fitting and Model Cross-Validation

The distance between the two farthest points of the soil layer entity at the entire site is 275 m. When calculating the variation function, the maximum search distance is greater than 160 m. It can meet the requirements of more than three sample points in the search distance. The exploration spacing is 20×20 m and the lag distance starts to fit the variogram from 10 m. After calculation, the fitting effect is optimal when the angle error limit is 22.5°. From the experimental variogram of characteristic directions of As, Mo, and Pb, the variogram with the smallest variance in the longest distance is selected as MAA. Figure 4 is the major axis of variogram curve fitting. The first line shows the major axis fitting results of As, Mo, and Pb in the entire soil layer, respectively. The four figures from the second row to the fourth row show the major axis fitting results of As, Mo, and Pb in the miscellaneous fill soil layer, silty clay layer, silty clay layer with gravel-sand, and gravel sand layer, respectively. After the major axis is determined, the plane perpendicular to the major axis is the plane where

SMA and MIA are located. Using the same method, the other two axes are obtained. After fitting with the ellipsoid, the parameters of an anisotropic ellipsoid (MAA/SMA, MAA/MIA, Azimuth: Bearing of MAA, Inclination angle: Plunge of MAA and dip of SMA) and the spherical model are obtained (Table 3).

From Table 3, it can be found that Mo and Pb have a high Nugget Effect, i.e., the ratio of nugget to sill is greater than 0.75, indicating that the spatial correlation between these two heavy metals is weak. This may be caused by random factors such as industrial pollution. Guedes *et al*. (2020) simulated the impact of different levels of Nugget Effect on Kriging valuation and noted that high Nugget Effect would negatively affect the efficiency of Kriging-based prediction. High Nugget Effect would negatively affect Kriging predictions and reduce the efficiency of Kriging-based spatial predictions. In the follow-up study, the efficiency of spatial interpolation prediction of Mo and Pb at this site should be further improved. The variation range of Pb in the gravel sand layer is 32.581 m and that of as in the miscellaneous fill layer is 102.13 m, indicating that the spatial variability of heavy metals is large.

Cross-validation provides an aggregated measure of error and allows the comparison of interpolation methods (Ouabo *et al*., 2020).ME, MAE, RMSE, and the proportion of errors in two standard deviations were used to verify the model parameters to assess the difference between the real and estimated values (Shen *et al*., 2019; Setiyoko *et al*., 2019). ME, MAE, and RMSE are close to 0. The error distribution should be normal and the confidence limit should be in the range of positive and negative double Kriging variance (Nasta *et al*., 2021). After cross-validation, the theoretical model parameters meet the cross-validation criteria and can be used for interpolation of As, Mo, and Pb at the site.
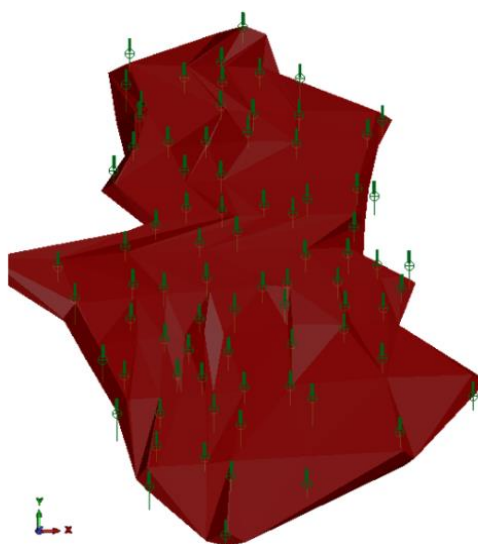

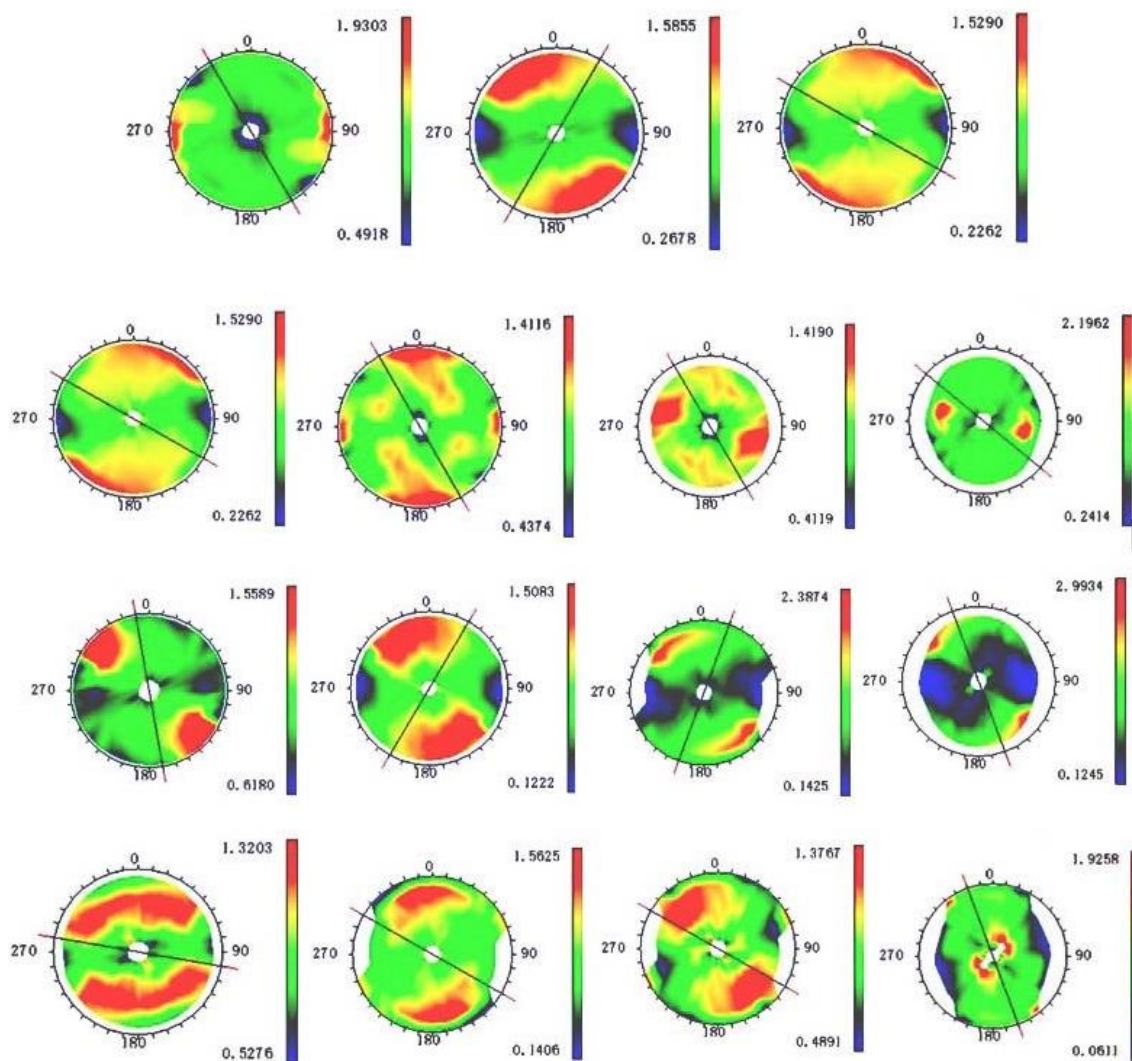**Fig. 3:** Three-dimensional solid model of the site

Fig. 4: Fitting results of spindle variogram

Table 2: Integrated sample statistics

Element	Stratum	Min/mgkg^{-1}	Max/mgkg^{-1}	Mean/mgkg^{-1}	Std.	Skew	Kur	Cv
As	1	7.40	65692.00	5247.00	10438.00	3.88	21.10	2.00
	2	6.20	23650.00	1548.00	3155.00	3.80	19.80	2.03
	3	7.26	10046.00	1012.00	1479.00	2.84	13.80	1.46
	4	7.86	4930.00	729.00	908.00	1.99	8.10	1.25
	5	2.50	65692.00	1700.00	4340.00	7.70	90.00	2.55
Mo	1	0.00	1856.00	66.00	214.00	6.20	47.60	3.24
	2	0.00	1567.00	25.00	107.00	10.70	144.60	4.19
	3	0.00	2640.00	32.00	204.00	10.37	119.00	6.40
	4	0.00	452.00	17.40	59.00	5.90	41.00	3.37
	5	0.00	2640.00	28.27	150.00	11.75	170.00	5.31
Pb	1	4.12	1560.00	209.00	395.00	2.90	11.76	1.90
	2	4.00	836.00	48.00	94.00	4.96	32.20	1.96
	3	3.30	512.40	32.90	46.00	5.31	45.40	1.40
	4	3.40	582.00	36.10	68.10	6.78	53.80	1.90
	5	3.30	1560.00	61.20	156.00	6.01	45.81	2.54

Note: 1. Miscellaneous fill 2. Silty clay 3. Silty clay with gravel sand 4. Gravel s and 5. Entire soil layer

229

Table 3: Parameters of anisotropic ellipsoid and spherical models

	Nugget value	Sill value	Nugget/ Sill	Range /m	MAA /SMA	MAA /MIA	Azimuth/°	Inclination angle/°	Dip angle/°
As	0.320	0.684	0.47	89.033	1.386	8.672	150	0	0
Mo	0.573	0.428	1.34	92.496	1.157	9.157	30	0	0
Pb	0.480	0.525	0.91	81.958	2.253	14.108	120	0	0
As (1)	0.443	0.558	0.79	102.13	1.473	15.390	160	0	0
As (2)	0.369	0.636	0.58	86.022	1.865	9.863	150	0	0
As (3)	0.338	0.663	0.51	87.076	1.040	11.469	150	0	0
As (4)	0.448	0.552	0.81	63.893	1.012	8.660	130	0	0
Mo (1)	0.535	0.465	1.15	52.753	1.221	6.852	170	0	0
Mo (2)	0.332	0.670	0.50	72.323	1.809	7.711	30	0	0
Mo (3)	0.224	0.780	0.29	83.764	1.011	10.096	20	0	0
Mo (4)	0.273	0.728	0.38	79.104	1.641	12.151	160	0	0
Pb (1)	0.532	0.469	1.13	98.367	2.164	11.894	100	0	0
Pb (2)	0.267	0.738	0.36	71.721	1.938	13.587	120	0	0
Pb (3)	0.482	0.519	0.93	65.549	1.115	5.725	120	0	0
Pb (4)	0.361	1.005	0.36	32.581	3.016	7.671	160	0	0

Note: As (1), As (2), As (3), and As (4) represent As is in the Miscellaneous fill soil layer, Silty clay layer, Silty clay layer with gravel-sand and Gravel sand layer, respectively. Mo (1), Mo (2), Mo (3), Mo (4) and Pb (1), Pb (2), Pb (3), and Pb (4) are the same

Discussion

The 3D-dimensional geological model divides the site into many small blocks. The concentration of pollutants in these small blocks is obtained by ordinary Kriging interpolation. The spatial distribution of pollutants at the site is analyzed and the polluted earthwork volume is estimated.

3D Visualization Analysis

Figure 5 shows the spatial distribution of As, Mo, and Pb pollution in the entire formation. The average concentration of As is 564.45 mg·kg⁻¹, far exceeding the control risk value of 60 mg·kg⁻¹. As is serious pollution, especially in the southwest of the site. The average concentration of Mo is 9.53 mg.kg⁻¹ and the proportion exceeding the control risk value of 775 mgkg⁻¹ is relatively small. The concentration of Mo in the northwest corner of the site is higher than in other areas. The average concentration of Pb is 35.40 mg.kg⁻¹ and the proportion exceeding the control risk value of 800 mg.kg⁻¹ is relatively small. There are multiple hotspots in its spatial distribution map and the highest risk areas are located southwest of the site.

The concentration of As, Mo, and Pb pollutants in the vertical direction gradually decreases from the surface layer to the lower layer (Fig. 6, 7, 8). The proportion of As in the miscellaneous fill soil layer greater than 1400 mg·kg⁻¹ is as high as 49.2%.

The arsenic production workshop is in the southwest area of the site. One of the reasons for serious pollution is the arsenic leakage in the production process. On the other hand, the dismantled production workshop was not protected in any way. Part of the construction waste was scattered on the ground and mixed with the soil and a large number of waste residues were piled up in the production workshop. The soil medium in this area has a good infiltration effect and rainwater leaching causes pollution. The terrain at the site is roughly high in the south and low in the north. Pollutants migrate in the soil due to rainwater leaching and ground washing water scouring. Pollutants are discharged with surface runoff to the lower north of the site, causing pollution in the north. According to the data, the groundwater depth of the site is relatively shallow (approximately 2.18-6.8 m). The pollutants in the shallow layer are leached with surface water and then seep, which easily causes the pollution of groundwater. Moreover, pollutants move vertically and horizontally with the flow of groundwater, resulting in deep soil and groundwater pollution in other areas. The lightly polluted area was a wasteland before the construction of the plant and no production activities were carried out. After the plant was built, the ground was hardened in this area, which had a certain preventive effect on soil pollution. Therefore, only the area close to the production workshop was polluted.

Due to the short production time of the molybdic acid plant, there is only a pollution risk around the molybdenum acid plant. The reason for the high Pb in the original roasting reverberatory furnace production workshop is that there is a small amount of Pb in the raw ore materials left after the workshop is closed. The waste residue dump area in the north may be because the waste residues contain Pb, which is piled on the surface of the site in the open air and has been leached and infiltrated by rainwater for a long time. Pb in the surrounding area of the ammonium molybdate plant may be affected by the northern waste residues.

Evaluation of Soil Heavy Metal Pollution

According to the soil pollution screening values, the single-factor index Pi and Nemerow comprehensive index

Pz of As, Mo, and Pb are calculated (Table 4-6). Pz of As in the entire soil layer is 228.62. It is a severely polluted area and heavy pollution (Pi>3) accounts for 63.70%. As accounts for 80.10% of the heavy pollution (Pi>3) of the miscellaneous fill, 61.10% of the heavy pollution (Pi>3) in silty clay, 3.6% of the heavy pollution (Pi>3) in silty clay with gravel-sand and 57.30% of the heavy pollution (Pi>3) with gravel sand. This shows that As is the most serious pollution in the miscellaneous fill soil layer. Pz of Mo in the entire soil layer is 0.2, which is the safety area. Pz of Pb in the miscellaneous fill soil layer is 0.7, which

is pollution prevention. The risk of potential pollution should be prevented and it is safe and non-polluting in other soil layers.

Contaminated Earthwork Volume

Based on the 3D-dimensional geological model, the earthwork volume under different pollution concentrations can be counted to provide a reference for the project cost in the future on-site management. Figure 9 is the earthwork volume of pollution at the site.
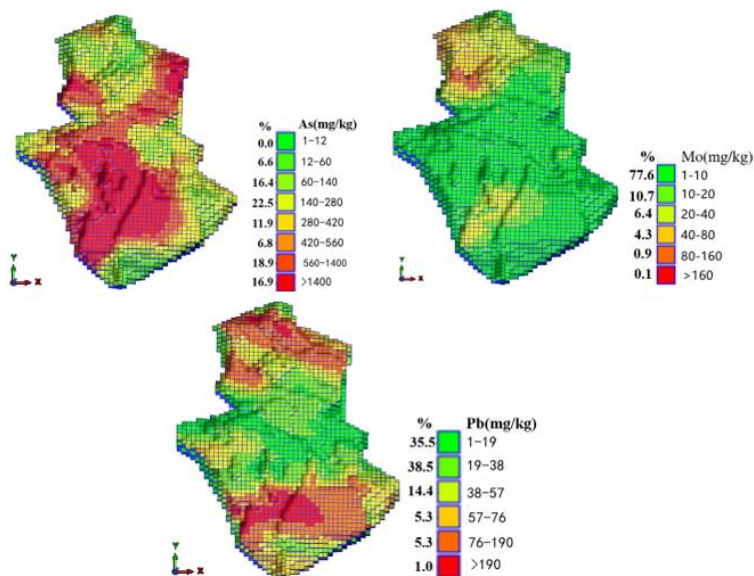
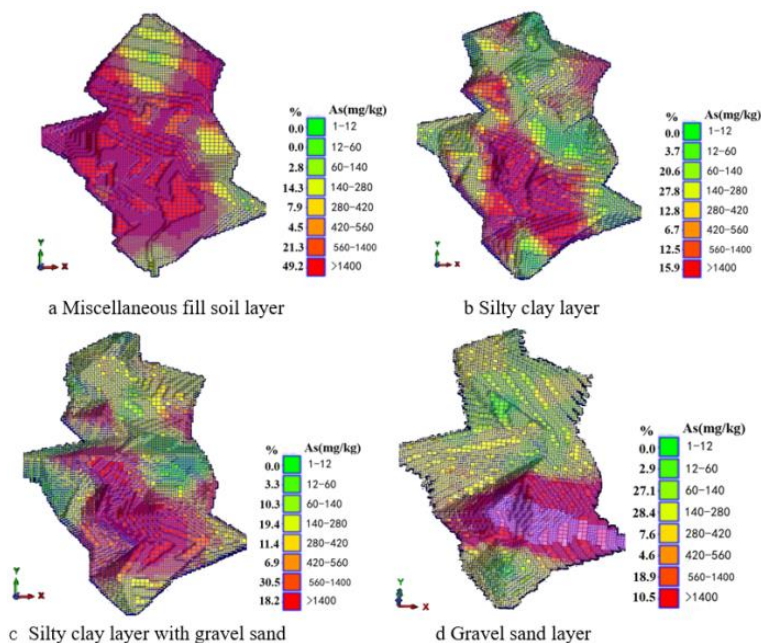**Fig. 5:** Stratigraphic interpolation results at the entire soil layer

a Miscellaneous fill soil layer

b Silty clay layer

c Silty clay layer with gravel sand

d Gravel sand layer

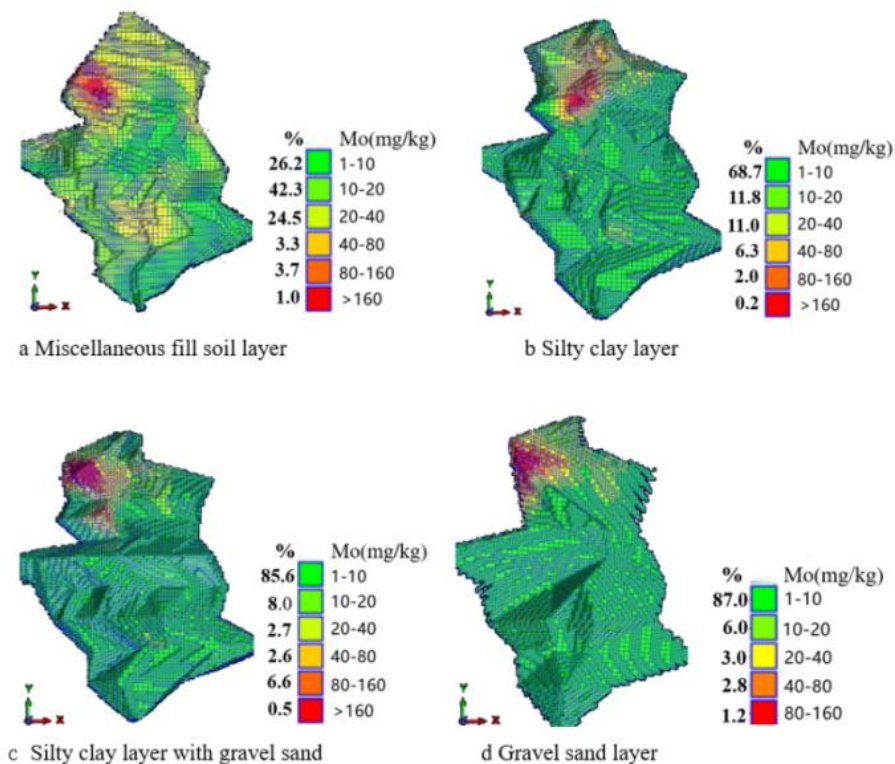**Fig. 6:** Distribution of as at each soil layer

231
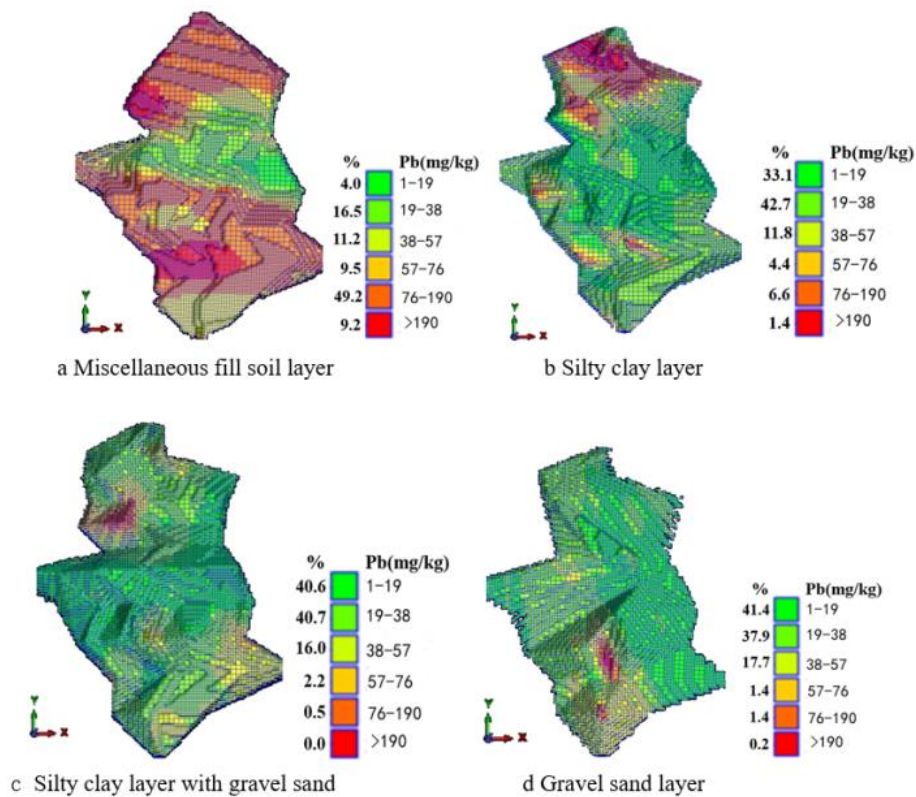
Fig. 7: Distribution of Mo at each soil layer

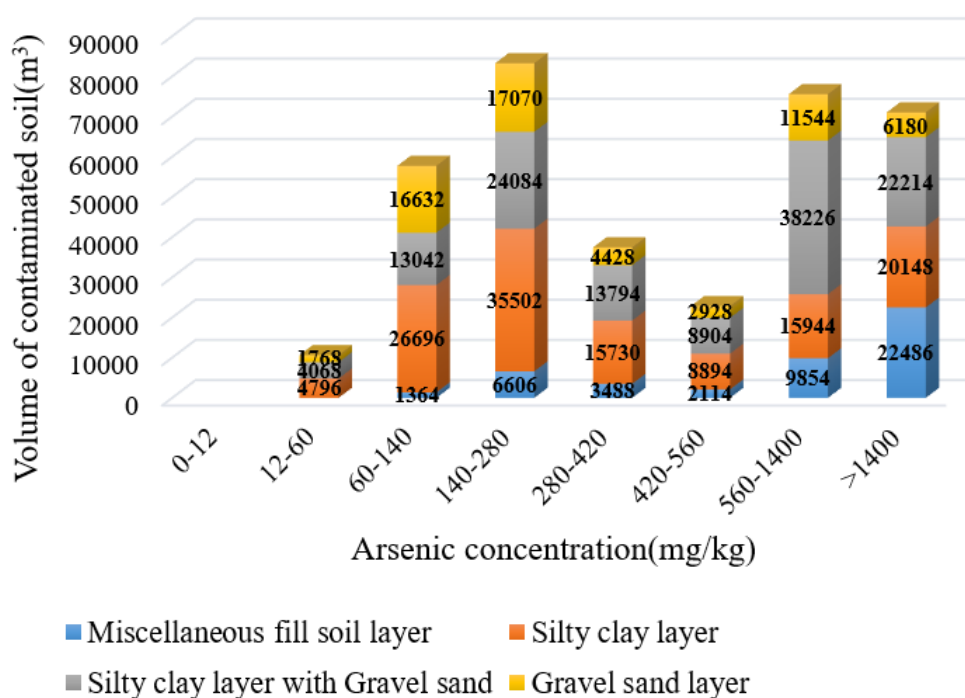**Fig. 8:** Distribution of Pb at each soil layer

Fig. 9: Earthwork contaminated by as at different concentrations

Table 4: Pi and Pz of As

| Element | The proportion of different pollution P_i/% | | | | | | | |
	$0<P_i\leq0.5$	$0.5<P_i\leq1$	$1<P_i\leq2$	$2<P_i\leq3$	$3<P_i\leq4$	$4<P_i\leq5$	$P_i>5$	P_z
5	8.80	5.90	11.20	10.40	10.10	7.70	45.90	228.62
1	14.60	0.00	2.50	2.60	3.00	2.60	74.50	148.27
2	19.30	1.00	6.70	11.90	11.00	10.80	39.30	133.15
3	3.50	1.50	9.50	12.00	10.90	9.00	53.70	77.92
4	2.20	0.20	15.70	24.70	16.90	9.70	30.70	24.56

Table 5: Pi and Pz of Mo

| Elements | Proportion of different pollution levels P_i/% | | | | | | | |
	$0<P_i\leq0.5$	$0.5<P_i\leq1$	$1<P_i\leq2$	$2<P_i\leq3$	$3<P_i\leq4$	$4<P_i\leq5$	$P_i>5$	P_z
5	100.00	0.00	0.00	0.00	0.00	0.00	0.00	0.16
1	100.00	0.00	0.00	0.00	0.00	0.00	0.00	0.21
2	100.00	0.00	0.00	0.00	0.00	0.00	0.00	0.21
3	100.00	0.00	0.00	0.00	0.00	0.00	0.00	0.61
4	100.00	0.00	0.00	0.00	0.00	0.00	0.00	0.14

Table 6: Pi and Pz of Pb

| Element | Proportion of different pollution levels P_i/% | | | | | | | |
	$0<P_i\leq0.5$	$0.5<P_i\leq1$	$1<P_i\leq2$	$2<P_i\leq3$	$3<P_i\leq4$	$4<P_i\leq5$	$P_i>5$	P_z
5	99.90	0.10	0.00	0.00	0.00	0.00	0.00	0.56
1	99.60	0.30	0.10	0.00	0.00	0.00	0.00	0.73
2	99.90	0.10	0.00	0.00	0.00	0.00	0.00	0.42
3	100.00	0.00	0.00	0.00	0.00	0.00	0.00	0.12
4	100.00	0.00	0.00	0.00	0.00	0.00	0.00	0.25

Conclusion

In this study, the soil heavy metal pollution of a site in Zhongshan, Guangxi was evaluated based on limited sampling points. The purpose is to emphasize the validity and importance of combining 3D geological modeling technology and geostatistical interpolation method to analyze the status of heavy metal pollution. The conclusions are as follows:

(1) Combining 3D geological modeling technology and the Kriging interpolation method to establish a 3D geological model of the polluted site can intuitively show the spatial distribution of heavy metals. The results show that the concentration of heavy metal pollutants at the site ranks as As>Pb>Mo. In the horizontal direction, the pollution is mainly concentrated in the southwest area of the site; in the vertical direction, the concentration of pollutants gradually decreases with the deepening of the soil layer, which intuitively shows the migration and diffusion law of pollutants in the underground. Based on the 3D geological model of the site, the earthwork volume of different concentrations of heavy metals can be easily estimated, which can provide a reference for the cost accounting in the future on-site governance

(2) The single-factor index and Nemerow comprehensive index are used to evaluate the heavy metal pollution at the site, which helps decision-makers to further clarify the remediation plan and screen there mediation technology. As is the most serious pollution and the medium and heavy pollution $(P_i>3)$ accounts for 61.10% of the entire soil layer, which will seriously threaten the local environmental safety. For Pb, it only needs to focus on its potential pollution risk in the mixed fill layer and the impact of Mo in the soil is in a safe range

In this way, 3D geological model helps analyze the law of heavy metal diffusion and can accurately describe the relationship between the spatial location and concentration of heavy metals to visually display the site pollution information. It also can provide a scientific basis for the subsequent restoration and governance of the site. In the future, the optimization of the combined model can be strengthened and the spatial distribution of pollutants can be simulated by using machine learning and deep learning technology to improve the interpolation accuracy and promote the intelligentization of environmental governance.

Funding Information

Author's Contributions

Baoshun Liu and Yonghong Zhang: Designed and performed the experiments, analyzed the data, and prepared the paper.

Jun Yao and Jian Su: Designed the experiments and revised the manuscript.

Ethics

The authors declare their responsibility for any ethical issues that may arise after the publication of this manuscript.

References

Abderrahmane, B., Naima, B., Tarek, M., & Abdelghani, M. (2021). Influence of Highway Traffic on Contamination of Roadside Soil with Heavy Metals. Civil Engineering Journal, 7(8), 1459-1471. file:///C:/Users/User/Downloads/2937-7922-1-PB.pdf

Agyeman, P. C., Ahado, S. K., Kingsley, J., Kebonye, N. M., Biney, J. K. M., Borůvka, L., ... & Kocarek, M. (2021). Source apportionment, contamination levels and spatial prediction of potentially toxic elements in selected soils of the Czech Republic. Environmental geochemistry and health, 43(1), 601-620. file:///C:/Users/User/Downloads/Agyeman_et_al-2020-Environmental_Geochemistry_and_Health.pdf

Ahado, S. K., Nwaogu, C., Sarkodie, V. Y. O., & Borůvka, L. (2021). Modeling and Assessing the Spatial and Vertical Distributions of Potentially Toxic Elements in Soil and How the Concentrations Differ. Toxics, 9(8), 181. file:///C:/Users/User/Downloads/toxics-09-00181-v2%20(1).pdf

Al-Mamoori, S. K., Al-Maliki, L. A., Al-Sulttani, A. H., El-Tawil, K., & Al-Ansari, N. (2021). Statistical analysis of the best GIS interpolation method for bearing capacity estimation in An-Najaf City, Iraq. Environmental Earth Sciences, 80(20), 1-14.file:///C:/Users/User/Downloads/Al-Mamoori2021_Article_StatisticalAnalysisOfTheBestGI.pdf

Barca, D., Bjosvik, L. L., Edman, G., Eliasson, U. H., Gervino, G., Philemark, C., & Svendson, B. D. (2021). Indoor Radon Concentration and Risk Estimation: The EURA PROJECT. Journal of Human, Earth and Future, 2(4), 323-333. file:///C:/Users/User/Downloads/87-275-1-PB.pdf

Barkat, A., Bouaicha, F., Bouteraa, O., Mester, T., Ata, B., Balla, D., ... & Szabó, G. (2021). Assessment of complex terminal groundwater aquifer for different use of Oued Souf Valley (Algeria) using multivariate statistical methods, geostatistical modeling and water quality index. Water, 13(11), 1609. file:///C:/Users/User/Downloads/water-13-01609.pdf

Belkhiri, L., Tiri, A., & Mouni, L. (2020). Spatial distribution of the groundwater quality using kriging and Co-kriging interpolations. Groundwater for Sustainable Development, 11, 100473. doi.org/10.1016/j.gsd.2020.100473

Breckenkamp, J., Razum, O., Spallek, J., Berger, K., Chaix, B., & Sauzet, O. (2021). A method to define the relevant ego-centered spatial scale for the assessment of neighborhood effects: The example of cardiovascular risk factors. BMC public health, 21(1), 1-7. file:///C:/Users/User/Downloads/Breckenkamp2021_Article_AMethodToDefineTheRelevantEgo-.pdf

Buaisha, M., Balku, S., & Özalp-Yaman, Ş. (2020). Heavy metal removal investigation in conventional activated sludge systems. Civil Engineering Journal, 6(3), 470-477. file:///C:/Users/User/Downloads/76c650bcce173763564518d4587f5b4b4839.pdf

Chaudhry, A. K., & Sachdeva, P. (2022). GIS-based groundwater quality assessment using GQIs and fuzzy-logic approach. Water and Environment Journal, 36(1), 172-182. doi.org/10.2166/ws.2019.111

Chen, G., Yang, Y., Liu, X., & Wang, M. (2021). Spatial Distribution Characteristics of Heavy Metals in Surface Soil of Xilinguole Coal Mining Area Based on Semivariogram. ISPRS International Journal of Geo-Information, 10(5), 290. file:///C:/Users/User/Downloads/ijgi-10-00290-v2.pdf

Choudhury, S. (2015). Comparative study on linear and non-linear geostatistical estimation methods: A case study on Iron deposit. Procedia Earth and Planetary Science, 11, 131-139. file:///C:/Users/User/Downloads/1-s2.0-S1878522015000685-main.pdf

Coulibaly, H. S. J. P., Honoré, C. T. J., Naga, C., Kouadio, K. C. A., DIDI, S. R. M., Diedhiou, A., & Savane, I. (2021). Groundwater exploration using extraction of lineaments from SRTM DEM and water flows in Béré region. The Egyptian Journal of Remote Sensing and Space Science, 24(3), 391-400. file:///C:/Users/User/Downloads/1-s2.0-S1110982320300867-main.pdf

Ćujić, M., Dragović, S., Đorđević, M., Dragović, R., & Gajić, B. (2017). Reprint of" Environmental assessment of heavy metals around the largest coal-fired power plant in Serbia". Catena, 148, 26-34. doi.org/10.1016/j.catena.2015.12.018

Fitriani, R., & Sumarminingsih, E. (2014). The dynamic of the spatial extent of land use in the fringe of Jakarta metropolitan: A semivariogram analysis. APCBEE procedia, 10, 198-202. file:///C:/Users/User/Downloads/1-s2.0-S2212670814001882-main.pdf

Gruszecka-Kosowska, A. (2019). Human health risk assessment and potentially harmful element contents in the fruits cultivated in southern Poland. International journal of environmental research and public health, 16(24), 5096. file:///C:/Users/User/Downloads/ijerph-16-05096.pdf

Guedes, L. P., Bach, R. T., & Uribe-Opazo, M. A. (2020). Nugget effect influences spatial variability of agricultural data. Engenharia Agrícola, 40, 96-104. file:///C:/Users/User/Downloads/download.pdf

Hasan, K., Paul, S., Chy, T. J., & Antipova, A. (2021). Analysis of groundwater table variability and trend using ordinary kriging: The case study of Sylhet, Bangladesh. Applied Water Science, 11(7), 1-12. file:///C:/Users/User/Downloads/Hasan2021_Article_AnalysisOfGroundwaterTableVari.pdf

Hou, D., O'Connor, D., Nathanail, P., Tian, L., & Ma, Y. (2017). Integrated GIS and multivariate statistical analysis for regional-scale assessment of heavy metal soil contamination: A critical review. Environmental Pollution, 231, 1188-1200. doi.org/10.1016/j.envpol.2017.07.021

Huang, H., Zhou, Y., Liu, Y., Li, K., Xiao, L., Li, M., ... & Wu, F. (2020). Assessment of Anthropogenic Sources of Potentially Toxic Elements in Soil from Arable Land Using Multivariate Statistical Analysis and Random Forest Analysis. Sustainability, 12(20), 8538. file:///C:/Users/User/Downloads/sustainability-12-08538-v2.pdf

Huang, S., & Xie, Y. L. (2019, May). Geostatistical estimation analysis of typical Carlin gold deposit in Hunan province, China. In IOP Conference Series: Earth and Environmental Science (Vol. 267, No. 2, p. 022033). IOP Publishing. file:///C:/Users/User/Downloads/Huang_2019_IOP_Conf._Ser.__Earth_Environ._Sci._267_022033.pdf

Kasmaee, S., Gholamnejad, J., Yarahmadi, A., & Mojtahedzadeh, H. (2010). Reserve estimation of the high phosphorous stockpile at the Choghart iron mine of Iran using geostatistical modeling. Mining Science and Technology (China), 20(6), 855-860. file:///C:/Users/User/Downloads/Reserve_estimation_of_the_high_phosphoro20160905-17709-1ukkvyk-with-cover-page-v2.pdf

Li, X., Li, D., Liu, Z., Zhao, G., & Wang, W. (2013). Determination of the minimum thickness of crown pillar for safe exploitation of a subsea gold mine based on numerical modeling. International Journal of Rock Mechanics and Mining Sciences, 57, 42-56. doi.org/10.1016/j.ijrmms.2012.08.005

Liu, G., Shi, Y., Guo, G., Zhao, L., Niu, J., & Zhang, C. (2020a). Soil pollution characteristics and systemic environmental risk assessment of a large-scale arsenic slag contaminated site. Journal of Cleaner Production, 251, 119721. doi.org/10.1016/j.jclepro.2019.119721

Liu, M., Hu, H., Wang, J. L., Zhang, L., Cheng, K., Cui, S.B. S., & Xue, J. (2020b). Investigation and evaluation of heavy metal pollution of crops around the coral mine and downstream areas in Zhongshan County, Guangxi. South China Geology and Minerals, (02), 169-176 (in Chinese with English abstract). doi.org/10.3969/j.issn.1007-3701.2020.02.009

Nasta, P., Szabó, B., & Romano, N. (2021) Evaluation of pedotransfer functions for predicting soil hydraulic properties: A voyage from regional to field scales across Europe. Journal of Hydrology: Regional Studies. 37:100903. doi.org/10.1016/j.ejrh.2021.100903

Nazzal, Y., Bărbulescu, A., Howari, F., Al-Taani, A. A., Iqbal, J., Xavier, C. M., ... & Dumitriu, C. Ș. (2021). Assessment of metals concentrations in soils of Abu Dhabi Emirate using pollution indices and multivariate statistics. Toxics, 9(5), 95. file:///C:/Users/User/Downloads/toxics-09-00095.pdf

O'Shea, M. J., Toupal, J., Caballero-Gómez, H., McKeon, T. P., Howarth, M. V., Pepino, R., & Gieré, R. (2021). Lead Pollution, Demographics and Environmental Health Risks: The Case of Philadelphia, USA. International journal of environmental research and public health, 18(17), 9055. file:///C:/Users/User/Downloads/ijerph-18-09055-v2.pdf

Othmani, M. A., Souissi, F., Durães, N., Abdelkader, M., & Da Silva, E. F. (2015). Assessment of metal pollution in a former mining area in the NW Tunisia: Spatial distribution and fraction of Cd, Pb and Zn in soil. Environmental Monitoring and Assessment, 187(8), 1-18. https://doi.org/10.1007/s10661-015-4734-9

Ouabo, R. E., Sangodoyin, A. Y., & Ogundiran, M. B. (2020). Assessment of ordinary Kriging and inverse distance weighting methods for modeling chromium and cadmium soil pollution in E-waste sites in Douala, Cameroon. Journal of Health and Pollution, 10(26). file:///C:/Users/User/Downloads/2156-9614-10_26_200605.pdf

Park, J., Kwon, E., Chung, E., Kim, H., Battogtokh, B., & Woo, N. C. (2019). Environmental sustainability of open-pit coal mining practices at Baganuur, Mongolia. Sustainability, 12(1), 248. file:///C:/Users/User/Downloads/sustainability-12-00248-v2.pdf

Qi, Z., Gao, X., Qi, Y., & Li, J. (2020). Spatial distribution of heavy metal contamination in mollisol dairy farm. Environmental Pollution, 263, 114621. doi.org/10.1016/j.envpol.2020.114621

Sabet Aghlidi, P., Cheraghi, M., Lorestani, B., Sobhanardakani, S., & Merrikhpour, H. (2020). Analysis, spatial distribution and ecological risk assessment of arsenic and some heavy metals of agricultural soils, case study: South of Iran. Journal of Environmental Health Science and Engineering, 18(2), 665-676. doi.org/10.1007/s40201-020-00492-x

Sampson, A. P., Weli, V. E., Nwagbara, M. O., & Eludoyin, O. S. (2021). Sensations of air temperature variability and mitigation strategies in urban environments. Journal of Human, Earth and Future, 2(2), 100-113. doi.org/10.28991/hef-2021-02-02-02

Santos-Francés, F., Martínez-Graña, A., Zarza, C. Á., Sánchez, A. G., & Rojo, P. A. (2017). Spatial distribution of heavy metals and the environmental quality of soil in the Northern Plateau of Spain by geostatistical methods. International journal of environmental research and public health, 14(6), 568. doi.org/10.3390/ijerph14060568

Sauzet, O., Breiding, J. H., Zolitschka, K. A., Breckenkamp, J., & Razum, O. (2021). An ego-Centred approach for the evaluation of spatial effects on health in urban areas based on parametric semi-Variogram models: Concept and validation. BMC medical research methodology, 21(1), 1-12. file:///C:/Users/User/Downloads/s12874-021-01300-2.pdf

Setiyoko, A., Arymurthy, A. M., & Basaruddin, T. (2019). DEM fusion concept based on the LS-SVM cokriging method. International Journal of Image and Data Fusion, 10(4), 244-262. doi.org/10.1080/19479832.2019.1664647

Setiyoko, A., Basaruddin, T., & Arymurthy, A. M. (2020). Minimax approach for semivariogram fitting in ordinary kriging. IEEE Access, 8, 82054-82065. file:///C:/Users/User/Downloads/Minimax_Approach_for_Semivariogram_Fitting_in_Ordinary_Kriging.pdf

Shen, Q., Wang, Y., Wang, X., Liu, X., Zhang, X., & Zhang, S. (2019). Comparing interpolation methods to predict soil total phosphorus in the Mollisol area of Northeast China. Catena, 174, 59-72. doi.org/10.1016/j.catena.2018.10.052

Tabesh, M., Vollmer, S., Schuettrumpf, H., & Frings, R. M. (2021). Spatial variability in river bed porosity determined by nuclear density gauging: A case study from a French gravel-bed river. Sedimentology.doi.org/10.1111/sed.12928

Tziachris, P., Metaxa, E., Papadopoulos, F., & Papadopoulou, M. (2017). Spatial modeling and prediction assessment of soil iron using kriging interpolation with pH as auxiliary information. ISPRS International Journal of Geo-Information, 6(9), 283. file:///C:/Users/User/Downloads/ijgi-06-00283.pdf

Van Dyke, M., Klemetti, T., &Wickline, J. (2020). Geologic data collection and assessment techniques in coal mining for ground control. International journal of mining science and technology, 30(1), 131-139. doi.org/10.1016/j.ijmst.2019.12.003

Wang, Y. Q., Bai, Y. R., & Wang, J. Y. (2014). Distribution of soil heavy metal and pollution evaluation on the different sampling scales in farmland on Yellow River Irrigation Area of Ningxia: A case study in Xingqing County of Yinchuan City. Huan Jing ke Xue = Huanjing Kexue, 35(7), 2714-2720. doi.org/10.3876/j.issn.1000-1980.2017.06.004

Xiang, Z., Gu, X., Wang, E., Wang, X., Zhang, Y., & Wang, Y. (2019). Delineation of deep prospecting targets by combining factor and fractal analysis in the Kekeshala skarn Cu deposit, NW China. Journal of Geochemical Exploration, 198, 71-81. doi.org/10.1016/j.gexplo.2018.12.004

Yan, T., Zhao, W., Zhu, Q., Xu, F., & Gao, Z. (2021). Spatial distribution characteristics of the soil thickness on different land-use types in the Yimeng Mountain Area, China. Alexandria Engineering Journal, 60(1), 511-520. doi.org/10.1016/j.aej.2020.09.024

Zhang, K., Li, X., Song, Z., Yan, J., Chen, M., & Yin, J. (2021). Human Health Risk Distribution and Safety Threshold of Cadmium in Soil of Coal Chemical Industry Area. Minerals, 11(7), 678. doi.org/10.3390/min11070678

Nomenclature

MAA	Major Axis of Anisotropic ellipsoid
SMA	Semi-Major Axis of the anisotropic ellipsoid
MIA	Minor Axis of the anisotropic ellipsoid
MAA/SMA	MAA to SMA ratio
MAA/MIA	MAA to MIA ratio
ME	Mean Error
MAE	Mean Absolute Error
RMSE	Root Mean Squared Error
Cv	Coefficient of variation
Std	Standard deviation